Ab initio nuclear momentum distributions in lithium hydride: Assessing nonadiabatic effects

Maciej Krzystyniak*
School of Science and Technology, Nottingham Trent University, Clifton Campus, Nottingham NG11 8NS, United Kingdom

Felix Fernandez-Alonso†
ISIS Facility, Rutherford Appleton Laboratory, Chilton, Didcot, Oxfordshire OX11 0QX, United Kingdom
(Received 15 December 2010; revised manuscript received 20 February 2011; published 29 April 2011)

Theoretical nuclear momentum distributions for solid lithium hydride and lithium deuteride are presented. Electronic-structure calculations were performed within the framework of plane-wave density functional theory, followed by the computation of phonon-dispersion relations and vibrational densities of states. The generalized-gradient-approximation functional of Perdew, Burke, and Ernzerhof was used in these first-principles calculations. Our computational results are compared with existing neutron Compton scattering and inelastic neutron scattering experiments on solid LiH. We find an excellent agreement between theory and experiment within the harmonic Born-Oppenheimer approximation. On the basis of the above, we estimate an upper conservative bound of ∼2 to 3% for the effects of nonadiabatic dynamics on the second moment and Laplacian of the atomic momentum distributions in this benchmark system. We close by discussing the implications of this study on future theoretical studies of atomic momentum distributions from isolated molecules and extended condensed-matter systems.

DOI: 10.1103/PhysRevB.83.134305 PACS number(s): 03.65.Yz, 03.65.Nk, 34.90.+q

I. INTRODUCTION

Neutron Compton scattering (NCS) is a unique method to investigate nuclear (single-particle) momentum distributions in molecules and condensed-matter systems.[1,2] In simple terms, NCS may be regarded as a mass-spectroscopic technique in which each atomic mass contributes to the overall time-of-flight (TOF) spectrum in the form of a Doppler-broadened recoil peak.[2] The width of such recoil peak in the energy domain can be then related to the kinetic-energy distribution in momentum space of the target nucleus prior to the scattering event. To date, calculations of atomic momentum distributions have been primarily carried out within the Born-Oppenheimer approximation (BOA).[2]

Owing to the ultrafast (attosecond) timescales associated with the NCS process as estimated by the Sears-Watson scattering time,[1,3] it has been suggested[4–6] that the celebrated BOA may not be fully applicable in proton-containing systems. In other words, during proton-neutron scattering, the recoiling proton has sufficient energy to mix electronic levels of the target system,[5] or proton-electron entanglement couples the dynamics of the recoiling proton and nearby electrons.[4,7] In this situation, the overall response function will contain additional spectral features arising from excited or nonstationary[4,7] electronic states of the target system.

To account for non-BOA contributions to proton momentum distributions, two independent models have been proposed by Gidopoulos[5] and by Reiter and Platzmann.[6] Both models are based on perturbative corrections to the proton recoil energy and predict the presence of extra NCS peaks centered at energy-transfer values higher than those corresponding to the proton recoil energy associated with the ground electronic state. These extra features manifest themselves as a broadening and/or shift of the center of gravity of the main proton recoil peak.[5,6]

In the simplified version of the Gidopoulos model, the high energies associated with proton recoil provide a mechanism for the participation of two electronic energy levels in the target system.[5] The efficiency of mixing of electronic states determines the extent to which the proton recoil peak is shifted or broadened. This quantity scales as the square root of the product of the proton recoil energy and the initial vibrational energy.[5] The Gidopoulos model applies to systems with a distinct energy separation between ground and excited electronic levels; otherwise, the perturbative approach breaks down. Thus, insulators with wide and well-defined electronic gaps are ideal candidates for experiments aimed at testing these theoretical predictions.

On an inverted-geometry NCS spectrometer like VESUVIO,[8] located at the ISIS Facility (Rutherford Appleton Laboratory, United Kingdom), the predictions of the Gidopoulos model would manifest themselves as a systematic discrepancy between experimental proton momentum distributions and theoretical predictions based on *ab initio* BOA calculations. The efficiency of mixing of electronic states, and, thus, the extent to which nuclear momentum distributions are distorted, can be compared for the case of two isoelectronic compounds exhibiting different recoil energies and different initial vibrational energies. Given the above, the most suitable test system is a simple insulator such as lithium hydride in protonated (LiH) and deuterated (LiD) forms. Moreover, due to the high symmetry of the LiH crystal structure (cubic, rock-salt-like), the mathematical description required to assess the nonadiabatic contributions to proton momentum distributions is greatly simplified compared to the general formalism introduced previously by Senesi *et al.*[9] These simple physical considerations constitute the main driving force behind the present paper.

Motivated by the above, we present *ab initio* calculations of proton momentum distributions in solid LiH and LiD in powder form. To this end, we have carried out plane-wave density-functional-theory (PW-DFT) computations using the generalized-gradient-approximation functional of Perdew, Burke, and Ernzerhof (GGA-PBE).[10] Nuclear momentum distributions are obtained via the computation of

phonon-dispersion relations and vibrational densities of states for face-centered-cubic (fcc) LiH and LiD crystals.

Our theoretical results for LiH are contrasted with available NCS and inelastic neutron scattering (INS) experiments on LiH powders.[11–13] A good agreement between theory and experiment is demonstrated within the harmonic BOA approximation. These computational results have important consequences for further theoretical modeling of nuclear momentum distributions in isolated molecules and condensed-matter systems.

This paper is organized as follows. First, the theory of NCS under the impulse approximation is briefly introduced. Then, the theoretical framework for the calculation of nuclear momentum distributions is presented for the case of a periodic lattice. Next, the details of the *ab initio* calculations are described with specific reference to crystalline LiH and LiD. The results of the *ab initio* calculations on solid LiH are then contrasted with previous NCS and INS experiments. We close by discussing the general implications of our results in future theoretical work on nuclear momentum distributions as measured by the NCS technique.

II. NEUTRON COMPTON SCATTERING IN THE IMPULSE APPROXIMATION

In NCS, the energy and momentum transfers imparted by the neutron to the target nucleus are so high that the scattering process can be treated within the impulse approximation (IA).[1–3,14–18] Within the IA, i.e., in the limit of infinite momentum transfer $\vec{q}$, the dynamic structure factor $S(\vec{q},\omega)$ reduces to a single peak centered at the recoil energy $\omega_r = \hbar^2 q^2/2M$ for a given nucleus of mass M. Consequently, we can write $S(\vec{q},\omega) = (M/\hbar^2 q)J(y)$, where y is the momentum $\vec{p}$ of the nucleus in the initial state projected onto the scattering vector $\vec{q}$. Mathematically, we can then write[3,19]

$$y = \vec{p}\cdot\hat{q} = \frac{M}{\hbar^2 q}(\omega - \omega_r) = \frac{M}{\hbar^2 q}\left(\omega - \frac{\hbar^2 q^2}{2M}\right), \quad (1)$$

where $\hat{q}$ is the unit vector in the direction of the momentum transfer. Hereinafter, momentum transfer will be given in units of Å^{-1}, energy transfer ω in meV, and atomic mass in amu. With this choice of units, Planck's constant is given by $\hbar$ = 2.04458 (meV amu)$^{1/2}$ Å.

$J(y,\hat{q})$ is the so-called Compton profile[1,3] and represents the longitudinal momentum distribution of the scattering nucleus along $\hat{q}$. For a harmonically bound isotropic system, where the momentum distribution $n(\vec{p})$ depends only on the magnitude of the radial momentum $|\vec{p}|$, $J(y,\hat{q}) = J(y)$. In the IA limit $J(y)$ can be written as a normalized Gaussian[2,14,17,18,20] of the form

$$J_{\rm IA}(y) = \frac{1}{\sqrt{2\pi\sigma_p^2}}\exp\left(\frac{-y^2}{2\sigma_p^2}\right), \quad (2)$$

where σ_p is the standard deviation.

For finite values of q, corrections to the IA are known as "final state effects" (FSEs).[2,18] To account for FSEs, the method of Sears[3] is routinely incorporated into standard NCS data treatments[18] by expressing the neutron Compton profile $J(y)$ as a series of the form

$$J(y) = J_{\rm IA}(y) - \frac{M\langle\nabla^2 V\rangle}{36\hbar^2 q}\frac{d^3}{dy^3}J_{\rm IA}(y) + \cdots, \quad (3)$$

where $J_{\rm IA}(y)$ is the IA result, and $\langle\nabla^2 V\rangle$ is the mean value of the Laplacian of the potential energy of the atom expressed in meV Å^{-2} (cf. Refs. 18,21).

In a realistic experimental situation, the total number of neutrons detected in an NCS spectrometer for a given mass M in a time-of-flight channel t is proportional to the Compton profile $J[y_M(t)]$, convoluted in y_M space with a (mass-dependent) instrumental resolution function $R[y_M(t)]$. Thus, for a total of N different masses present in the sample, the total count rate at a fixed scattering angle θ, $C_\theta(t)$, is given by [cf. Ref. 18, Eq. (2.24)]

$$C_\theta(t) = A'\left[\frac{E_0 I(E_0)}{q}\right]_t \times \sum_{n=1}^{N} I_n M_n J_n[y_n(t)] \otimes R_n[y_n(t)], \quad (4)$$

where A' is a mass-independent experimental constant, and the mass-independent factor $[\frac{E_0 I(E_0)}{q}]_t$ depends on the incident neutron spectrum $I[E_0(t)]$, the initial neutron energy $E_0(t)$, and the momentum transfer $q(t)$, all functions of the time of flight t (Ref. 18). In Eq. (4), the nuclear momentum distribution of mass M, $J_M(y_M(t))$, is given by Eq. (3). Integrated peak intensities I_M for a given scattering center of mass M are proportional to the scattering density $I_M = AN_M\sigma_M$, where $\sigma_M = 4\pi b_M^2$ is the total (bound) neutron scattering cross section.[18,22]

III. NUCLEAR MOMENTUM DISTRIBUTION FOR MOLECULAR MOTIONS IN A PERIODIC LATTICE

Nuclear momentum distributions in a regular solid are most conveniently accounted for on the basis of the projected vibrational density of states in a periodic lattice. A number of approximations are made in order to arrive at a phonon description of lattice vibrations. First of all, it is assumed that the mean equilibrium position of each atom, i, corresponds to a Bravais lattice site $\vec{R}_i$. Second, it is assumed that the amplitude of atomic displacements is small compared to interatomic distances, naturally leading to the harmonic approximation for atomic displacements.[23,24] With these approximations in mind, a phonon-based description of the vibrational properties of the crystal only requires knowledge of one fundamental quantity, namely, the force-constant matrix (FCM)[23,24]

$$D_{\mu\nu}(\vec{R} - \vec{R}') = \left.\frac{\partial^2 E}{\partial u_\mu(R)\partial u_\nu(R')}\right|_{u=0}, \quad (5)$$

where u refers to the displacement of a given atom from its equilibrium position, and E is the total energy within the harmonic approximation. The FCM can also be represented

in reciprocal space, which is commonly referred to as the dynamical matrix (DM)

$$D_{\mu\nu}(\vec{q}) = \frac{1}{N_R} \sum_{\vec{R},\vec{R}'} D_{\mu\nu}(\vec{R} - \vec{R}') \exp[-i\vec{q}(\vec{R} - \vec{R}')], \quad (6)$$

where N_R is the number of Bravais lattice sites.

With these definitions, equations of motion can be written in the language of dynamical matrices as an eigenvalue problem. Each atomic displacement is described as a plane wave of the form

$$\vec{u}(\vec{R},t) = \vec{e}(\vec{q}) \exp[-i\vec{q}\,\vec{R} - \omega(\vec{q})t], \quad (7)$$

where the polarization vector of each mode, $\vec{e}(\vec{q})$, is an eigenvector of a $3N$-dimensional eigenvalue problem describing all possible vibrational modes. The eigenvalue equation reads

$$M\omega(\vec{q})^2\,\vec{e}\,(\vec{q}) = D(\vec{q})\,\vec{e}\,(\vec{q}). \quad (8)$$

Phonon dispersion relations are obtained by mapping the wave vector ($\vec{q}$) dependence of the frequency eigenvalues $\omega(\vec{q})$.

In density functional perturbation theory (DFPT) calculations, we seek to evaluate the dynamical matrix directly for a set of q-vectors.[23–25] Due to the variational nature of the DFT formalism, the DFPT problem can be solved by minimizing the second-order perturbation in the total energy, yielding first-order variations to the electronic density, wave functions, and potential.

In the following, we shall assume that the momentum distribution of the n^{th} nucleus in a crystal along the $\hat{q}$ direction assumes a purely multivariate Gaussian functional form. This "Gaussian" approximation (GA) has already been demonstrated to work very well in crystalline HCl.[9] In essence, the GA reflects the essentially harmonic nature of the potential energy surface in the vicinity of the equilibrium position where the vibrational wave function is necessarily of Gaussian form. In this case, the second-moment of the momentum distribution for a given nucleus n and along a given direction $\hat{q}$, $\sigma_n^2(\hat{q})$, can be written as

$$\sigma_n(\hat{q})^2 = \frac{M_n}{N_q\hbar^2} \sum_{q\in 1BZ} \sum_{\lambda=1}^{N_\lambda=12} [\vec{e}_n(\lambda,\vec{q}) \cdot \hat{q}]^2 \times \frac{\omega(\lambda,\vec{q})}{2} \coth\left(\frac{\omega(\lambda,\vec{q})}{2k_BT}\right), \quad (9)$$

where $\omega(\lambda,\vec{q})$ are phonon frequencies, and $\vec{e}_n(\lambda,\vec{q})$ are polarization vectors for a given nucleus n. The summation in Eq. (9) runs over all q vectors contained in the first Brillouin zone, where N_q is the number of these wave vectors, as well as over the twelve phonon branches λ of the fcc unit cell of relevance to this paper.

From Eq. (9), the spherically averaged value of the second moment of the nuclear momentum distribution for a nucleus n, $\sigma_{Mn}(\hat{q})^2$, can be obtained using two different routes. In the first route, the spherical average is calculated analytically from Eq. (9) using the following expression[26]

$$\sigma_n^2 = \tfrac{1}{3}[\sigma_n(\hat{x})^2 + \sigma_n(\hat{y})^2 + \sigma_n(\hat{z})^2]. \quad (10)$$

In the second route, the total vibrational density of states projected onto nucleus n, $G_n(\omega)$, is used to compute $\sigma_{Mn}(\hat{q})^2$ explicitly using the relation

$$\sigma_n^2 = \frac{M_n}{\hbar^2} \int G_n(\omega) \frac{\omega}{2} \coth\left(\frac{\omega}{2k_BT}\right) d\omega. \quad (11)$$

The partial phonon density of states, $G_n(\omega)$, is determined as the contribution from a given atom to the total phonon density of states. $G_n(\omega)$ is defined by the following sum over all q points in the first Brillouin zone and over all phonon bands[27,28]

$$G_n(\omega) = \frac{1}{3N_q} \sum_{\vec{q}\in 1BZ} \sum_{\lambda=1}^{N_\lambda=12} \vec{e}_n(\lambda,\vec{q})^2 \delta[\omega - \omega(\lambda,\vec{q})], \quad (12)$$

where $\vec{e}_n(\lambda,\vec{q})$ are the polarization vectors for phonon modes λ of energy $\omega(\lambda,\vec{q})$, and N_q is the number of points in the first Brillouin zone.

The partial phonon density of states, $G_n(\omega)$, for a harmonic solid can also be used to estimate the magnitude of FSEs introduced in Eq. (3). The spherical average of the Laplacian of the local effective potential felt by nucleus n can be expressed as[29]

$$\langle \nabla^2 V_n \rangle = \frac{3M}{\hbar^2} \int \omega^2 G_n(\omega) d\omega. \quad (13)$$

For an isotropic three-dimensional harmonic oscillator (3D-HO), we can assume for the vibrational density of states

$$G_n(\omega) = \delta(\omega - \omega_0), \quad (14)$$

where ω_0 is its characteristic energy corresponding to the ground vibrational state of the 3D-HO. Using the virial theorem, we get

$$\frac{\omega_0}{4} = \langle E_k \rangle = \frac{\hbar^2}{2M} \langle \sigma^2 \rangle. \quad (15)$$

Thus, Eq. (13) yields for the special case of a 3D-HO oscillator[18]

$$\langle \nabla^2 V \rangle = \frac{12\hbar^2\sigma^4}{M}. \quad (16)$$

Plugging the above term $\frac{12\hbar^2\sigma^4}{M}$ from Eq. (16) into the Sears' FSE factor, $\frac{M\langle\nabla^2 V\rangle}{36\hbar^2 q}$ [cf. Eq. (3)], we get

$$\frac{M\langle \nabla^2 V \rangle}{36\hbar^2 q} = \frac{\sigma^4}{3q}. \quad (17)$$

Using Eq. (2) for $J_{\text{IA}}(x)$ with $x = \frac{y}{\sqrt{2\sigma^2}}$, taking its third derivative with respect to y, $\frac{d^3}{dy^3} J_{\text{IA}}(x)$, and using the definition of the third-order Hermite polynomial, $H_3(x) = 8x^3 - 12x$, leads to

$$\frac{M\langle \nabla^2 V \rangle}{36\hbar^2 q} \frac{d^3}{dy^3} J_{\text{IA}}(x) = \frac{\sigma}{q} \frac{\sqrt{2}}{12} H_3(x) J_{\text{IA}}(x). \quad (18)$$

By rewriting Eq. (3) using

$$J_{\text{FSE}}(x) = -\frac{k}{q} H_3(x) J_{\text{IA}}(x), \quad (19)$$

we get an explicit connection between the parameter k and the standard deviation of the nuclear momentum distribution σ for the case of a harmonically bound nucleus, namely,

$$k = \sigma \frac{\sqrt{2}}{12}. \tag{20}$$

Equation (20) is useful in the analysis of measured nuclear momentum distributions using the Gram-Charlier expansion. In this case, the parameter k can be relaxed during the fitting procedure and then compared with a prediction based on a purely harmonic system. Also, a comparison of the spherical average of the Laplacian of the effective Born-Oppenheimer potential experienced by the nuclei as obtained from our *ab initio* calculations [cf. Eq. (13)] with the value calculated in the limit of an isotropic three-dimensional harmonic potential [cf. Eq. (16)] allows us to assess the validity of the harmonic approximation in specific situations.

Using the expression for the partial density of states given by Eq. (12) and plugging it back into Eq. (13) for the spherical average of the Laplacian of the effective potential felt by nucleus n yields an expression for the Laplacian in terms of polarization vectors $\vec{e}_n(\lambda,\vec{q})$:

$$\langle \nabla^2 V_n \rangle = \frac{M_n}{N_q \hbar^2} \sum_{q \in 1BZ} \sum_{\lambda=1}^{N_\lambda=12} \langle \vec{e}_n(\lambda,\vec{q})^2 \rangle \omega(\lambda,\vec{q})^2. \tag{21}$$

Moreover, recalling that

$$\langle \nabla^2 V_n \rangle = \frac{1}{3} \left(\frac{\partial^2 V_n}{\partial x^2} + \frac{\partial^2 V_n}{\partial y^2} + \frac{\partial^2 V_n}{\partial z^2} \right) \tag{22}$$

and

$$\langle (e_n(\lambda)^2 \rangle = \tfrac{1}{3} [e_n(\lambda,\hat{x})^2 + e_n(\lambda,\hat{y})^2 + e_n(\lambda,\hat{z})^2] \tag{23}$$

leads us to

$$\frac{\partial^2 V_n}{\partial u^2} = \frac{M_n}{N_q \hbar^2} \sum_{q \in 1BZ} \sum_{\lambda=1}^{N_\lambda=12} \vec{e}_n(\lambda,\hat{u})^2 \omega(\lambda,\vec{q})^2, \tag{24}$$

where $\hat{u} = \{\hat{x},\hat{y},\hat{z}\}$.

Equation (24) provides a useful recipe for the *ab initio* modeling of the anisotropy of the effective Born-Oppenheimer potential from phonon-dispersion relations in both molecules and condensed-matter systems.

IV. *AB INITIO* CALCULATION OF PROTON MOMENTUM DISTRIBUTIONS

The nuclear momentum distributions in solid LiH and LiD were calculated from the phonon-dispersion relations and vibrational density of states in a periodic lattice using the PW-DFT approach. The PW-DFT software package CASTEP,[30,31] developed by the UK Carr-Parrinello Consortium, was used throughout this paper. CASTEP was run on the SCARF supercomputing cluster at the Rutherford Appleton Laboratory, United Kingdom. The input and output preparation for the PW-DFT calculation in CASTEP was performed with the MATERIALS STUDIO program supplied by ACCELRYS. *Ab initio* calculations of nuclear momentum distributions were performed in two sequential steps, namely, an initial geometry optimization, followed by the calculation of vibrational properties for a cubic crystal cell as shown in Fig 1. The GGA[32] functional of Perdew, Burke, and Ernzerhof functional was used, which is a usual choice for strongly interacting hydrogenous systems.[33,34] Core electrons were represented as norm-conserving pseudopotentials. The electronic wave functions were expanded in a plane-wave basis set with a cutoff of 750 eV. The sampling of the Brillouin zone was performed on a $6 \times 6 \times 6$ k-point grid which was reduced by symmetry to 10 special k points. Electronic-energy minimization was performed with a convergence tolerance of 0.2×10^{-5} eV/atom.

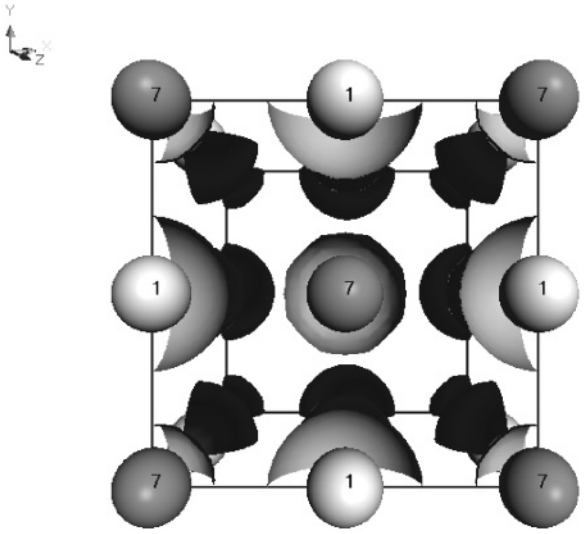

FIG. 1. LiH cubic cell employed in the calculations. The numbers indicate the atomic masses for Li(7) and H(1). An identical geometry was used for LiD.

The electronic band structure and the electronic density of states for the optimized LiH geometry are shown in Fig. 2. From Fig. 2, it is apparent that there is a band gap in the LiH electronic band structure of ca. 2.99 eV at the Γ point of the Brillouin zone. This value is very similar to the value of 3.00 eV obtained by van Setten *et al.*[35] It is known that PW-DFT can underestimate band gaps, with GGA giving considerably smaller values than 4.5–4.6 eV, as obtained with projector-augmented-wave (PAW) methods (Ref. 35). Also, the dynamically screened-interaction approximation (GWA) used to generate single-particle excitation energies within the quasiparticle (QP) approximation, having as a starting point the local-density approximation (LDA), gives considerably higher values to the band gap in LiH. These lie in the range 4.6–5.4 eV, much closer to the experimental value of 4.99 eV.[35]

Geometry optimization was performed with the Broyden-Fletcher-Goldfarb-Shanno (BFGS) algorithm with a total-energy convergence tolerance of 0.2×10^{-4} eV/atom, a maximum ionic-force tolerance of 0.5×10^{-1} eV/Å, and a maximum ionic-displacement tolerance of 0.2×10^{-2} Å. The optimized geometry corresponded to a cubic unit cell of dimensions $a = b = c = 4.022$ Å. This result is very close to the result $a = b = c = 4.02$ Å, obtained by van Setten *et al.* using a similar PW-DFT GGA approach.[35] These values are somewhat smaller than the experimental lattice parameters of 4.09 Å[36] owing to the neglect of zero-point-energy motions in our geometry optimization.[37,38]

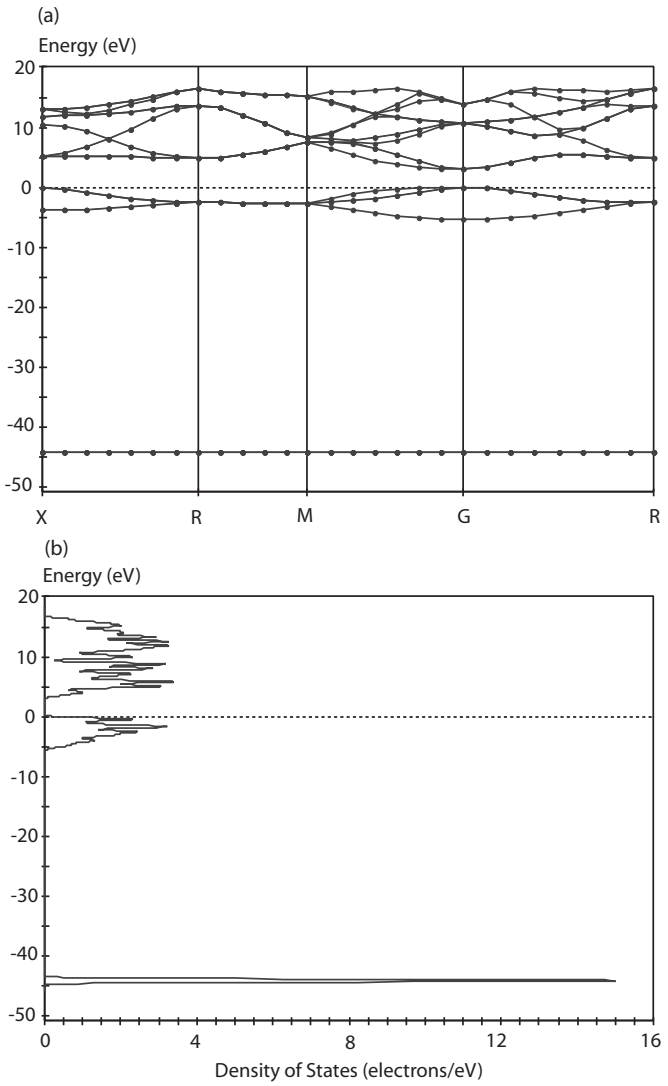

FIG. 2. (a) Electronic band structure and (b) electronic density of states for an fcc cubic LiH crystal. A pronounced band gap of 2.992 eV at the γ point is clearly visible in these data.

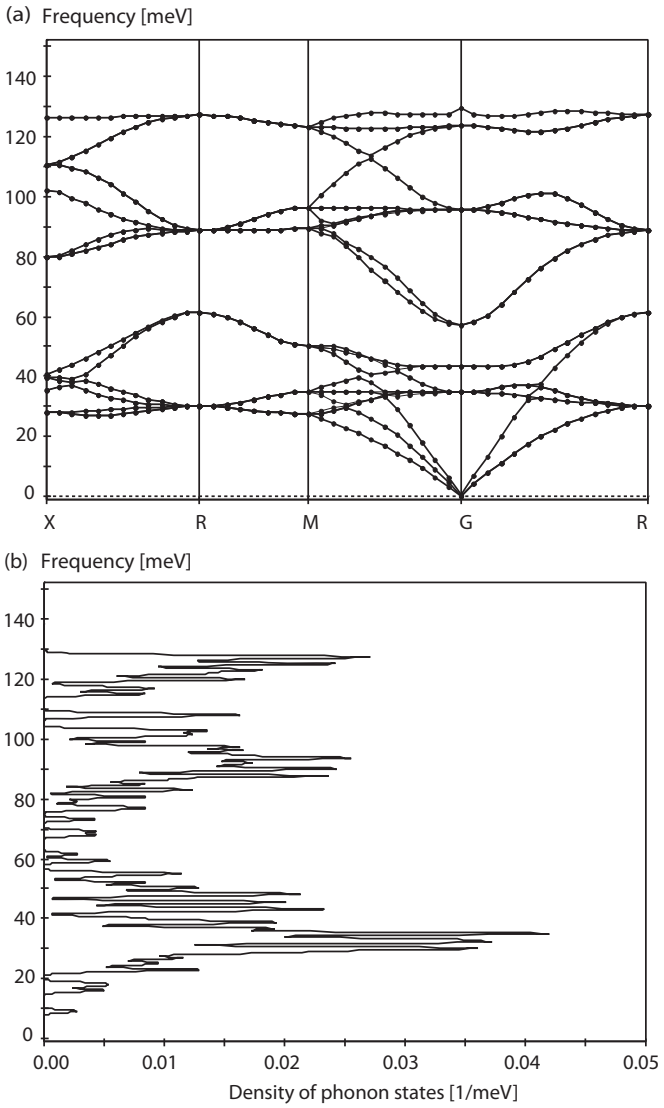

FIG. 3. (a) LiH phonon dispersion and (b) total phonon density of states.

For insulating materials, the CASTEP package supports phonon calculations within the framework of linear response theory, with the core electrons represented as norm-conserving pseudopotentials.[30,31] Following this approach, phonon calculations were performed in CASTEP at 28 wave vectors including acoustic sum-rule corrections. The phonon convergence tolerance for the calculation was set to 10^{-5} eV/Å^2, and the band convergence tolerance to 10^{-9} eV. From the phonon-dispersion relations, total and partial (projected) vibrational densities of states were also calculated for LiH (Figs. 3 and 4) and LiD (Figs. 5 and 6).

From the simulated phonon-dispersion data within the first Brillouin zone (1BZ), $F(\omega,\vec{q} \in 1\text{BZ})$, phonon frequencies $\omega(\lambda,\vec{q} \in 1\text{BZ})$, and polarization vectors $\vec{e}_n(\lambda,\vec{q} \in 1\text{BZ})$ were numerically calculated for all 12 phonon branches over the entire q grid. The widths σ_{Mn} of the nuclear momentum distributions along each Cartesian direction (cf. Fig. 1) were calculated using Eq (9). Finally, the isotropic average was performed for each nucleus within the unit cell using Eq. (10). As a check of these calculations, the isotropic average of the width of the momentum distribution, σ_n, calculated using Eq. (11) was also compared to the value obtained from Eq. (9).

The standard deviations of the nuclear momentum distributions, σ_M, along the x, y, and z directions for LiH and LiD are reported in Tables I and II, respectively. The values of σ_M were calculated for two distinct temperatures, 20K and 300K, using Eq. (9). The average isotropic widths calculated using Eq. (10) are compared to values obtained using Eq. (11) as first and second entries in the last columns of the tables, respectively. It is worth mentioning that the calculation yields values for the widths of the nuclear momentum distributions that are the same to within 1 to 2% for all identical nuclei within the LiH and LiD unit cells, as one would expect on the grounds of the cubic symmetry of this material.

Table III lists our theoretical predictions for H and Li nuclei in LiH and LiD at 20 K and 300 K. These values have been obtained using the *ab initio* vibrational densities of states and

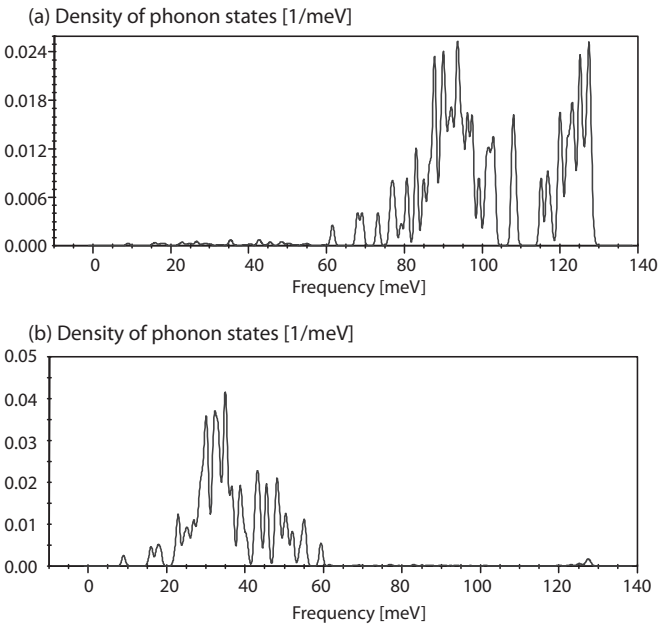

FIG. 4. Partial vibrational density of states in LiH. (a) H projected and (b) Li projected.

Eq. (11), and correspond to the average kinetic energy and the square root of the second moment of the nuclear momentum distribution.

Table IV lists the theoretical values for H and Li atoms in LiH and LiD corresponding to the (x,y,z) components of the Laplacian of the effective Born-Oppenheimer (BO) potential [cf. Eq. (24)]. In addition, we also report the spherical average of the Laplacian, $\langle \nabla^2 V \rangle$, obtained from the phonon-dispersion relations [cf. Eq. (21)] and from the vibrational density of states [cf. Eq. (13)]. A comparison of the latter two values provides a sound consistency check for the validity of our *ab initio* calculations for both LiH and LiD. In both LiH and LiD, the components of the Laplacian along all crystallographic directions do not differ from the spherical average by more than 5%. Thus, the effective BO potential experienced by the nuclei can be considered to be predominantly isotropic within the accuracy of the present calculations.

TABLE I. Standard deviations σ_M of the nuclear momentum distribution along x, y, and z for all nuclei in the LiH cubic cell using Eq. (9). The average isotropic widths have been calculated using Eq. (10).

	$\sigma_M(\hat{x})$ [Å^{-1}]		$\sigma_M(\hat{y})$ [Å^{-1}]		$\sigma_M(\hat{z})$ [Å^{-1}]		$\overline{\sigma_M}$ [Å^{-1}]	
Nucleus	20 K	300 K	20 K	300 K	20 K	300 K	20 K	300 K
H1	3.53	3.60	3.39	3.57	3.44	3.53	3.49	3.57
H2	3.53	3.60	3.39	3.57	3.44	3.53	3.49	3.57
H3	3.53	3.60	3.39	3.57	3.44	3.53	3.49	3.57
H4	3.53	3.60	3.39	3.57	3.44	3.53	3.49	3.57
Li1	5.66	7.18	5.60	7.15	5.51	7.10	5.59	7.14
Li2	5.66	7.18	5.60	7.15	5.51	7.10	5.59	7.14
Li3	5.66	7.18	5.60	7.15	5.51	7.10	5.59	7.14
Li4	5.66	7.18	5.60	7.15	5.51	7.10	5.59	7.14

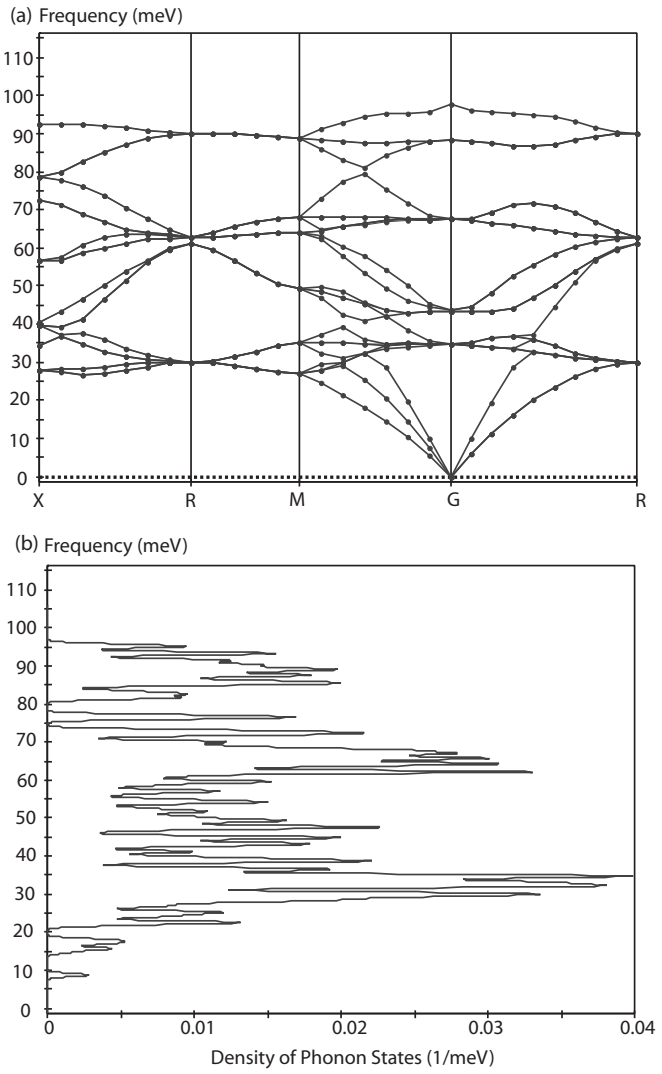

FIG. 5. (a) LiD phonon dispersion and (b) total phonon density of states.

Table V lists the experimental values obtained for protons in LiH from NCS experiments at 20 K and 300 K on the VESUVIO NCS spectrometer,[39] as well as INS measurements on the TOSCA inelastic neutron spectrometer,[40] also located at the ISIS Facility, Rutherford Appleton Laboratory, United Kingdom. These data include average kinetic energies $E_{\rm kin}$, the square root of the second moment of the momentum distribution, σ (calculated from $E_{\rm kin}$), and the spherical average of the Laplacian of the effective Born-Oppenheimer potential, $\langle \nabla^2 V \rangle$, calculated within the isotropic 3D-HO approximation using Eq. (16).

From Table V, it is apparent that PW-DFT *ab initio* calculations using vibrational densities of states within the harmonic approximation provide good estimates of the experimental values for both the kinetic energy and the square root of the second moment of the proton momentum distribution in solid LiH. The value of $\sigma_H = 3.57$ Å^{-1} in LiH obtained from our *ab initio* calculations at $T = 300$ K is only $\sim$2% larger than 3.49 ± 0.05 Å^{-1}, the isotropic average value obtained from previous NCS measurements at the same temperature (Refs. 12,40). Most interestingly, the *ab initio* value of σ_H at

TABLE II. Standard deviations σ_M of the nuclear momentum distribution along x, y, and z for all nuclei in the LiD cubic cell using Eq. (9). The average isotropic widths have been calculated using Eq. (10).

Nucleus	$\sigma_M(\hat{x})$ [Å^{-1}] 20 K	300 K	$\sigma_M(\hat{y})$ [Å^{-1}] 20 K	300 K	$\sigma_M(\hat{z})$ [Å^{-1}] 20 K	300 K	$\overline{\sigma_M}$ [Å^{-1}] 20 K	300 K
D1	4.19	4.47	4.15	4.44	4.09	4.39	4.14	4.43
D2	4.19	4.47	4.15	4.44	4.09	4.39	4.14	4.43
D3	4.19	4.47	4.15	4.44	4.09	4.39	4.14	4.43
D4	4.19	4.47	4.15	4.44	4.09	4.39	4.14	4.43
Li1	5.69	7.18	5.62	7.15	5.52	7.10	5.61	7.15
Li2	5.69	7.18	5.62	7.15	5.52	7.10	5.61	7.15
Li3	5.69	7.18	5.62	7.15	5.52	7.10	5.61	7.15
Li4	5.69	7.18	5.62	7.15	5.52	7.10	5.61	7.15

$T = 20$ K, 3.49 Å^{-1}, is bracketed by previous experimental values for σ_H, namely, 3.44 Å^{-1} (NCS measurements)[12] and 3.59 Å^{-1} (INS measurements).[40]

Also, the *ab initio* values of the isotropically averaged Laplacians of the effective Born-Oppenheimer potentials in LiH, $\langle\nabla^2 V\rangle$, agree well with those derived from NCS and INS experiments assuming an isotropic 3D-HO model. A theoretical value of $\langle\nabla^2 V\rangle$=7622 meV Å^{-2} for H in LiH is also bracketed by experimental values of 6968 and 8265 meV Å^{-2},[39,40] and it is only 3% higher than the value measured in NCS experiments at 300 K.[39]

V. DISCUSSION

Nuclear momentum distributions were calculated quantum mechanically based on a PW-DFT approach for the optimized cubic LiH and LiD crystal cells. The GGA-PBE functional[10] was used in these calculations. Our predictions include the

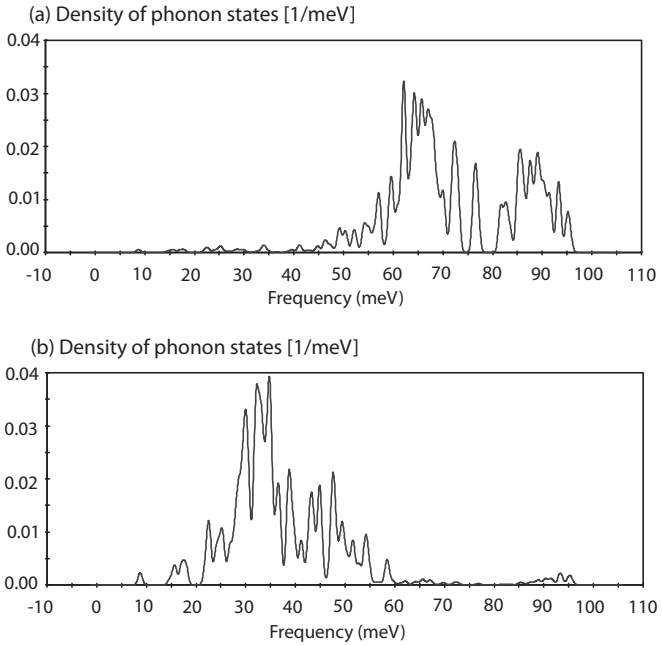

FIG. 6. Partial vibrational density of states in LiD. (a) D projected and (b) Li projected.

TABLE III. Average kinetic energy and square root of the second moment of the nuclear momentum distribution for H and Li in LiH and LiD.

Nucleus	E_{kin} [meV] 20 K	300 K	σ [Å^{-1}] 20 K	300 K
H in LiH	75.8	79.4	3.49	3.57
Li in LiH	28.1	45.9	5.57	7.13
D in LiD	53.4	61.2	4.14	4.43
Li in LiD	28.2	45.9	5.59	7.13

second moment σ of the momentum distribution as well as the Laplacian $\langle\nabla^2\rangle$ of the effective Born-Oppenheimer potential along all crystallographic directions. Given its small number of electrons, lithium hydride has been a popular system for the benchmarking of various DFT approaches in the prediction of phonon densities of states and dispersion relations. Recently, state-of-the-art calculations have been performed by Barrera *et al.*[38] The authors performed *ab initio* electronic-structure calculations on several alkali-metal hydrides using both the LDA and the GGA. The quasiharmonic approximation was used where the Helmholtz energy of a crystal at a given temperature represents the sum of the potential energy of the static lattice and harmonic vibrational contributions associated with atomic motions. For the alkali-metal hydrides (including LiH), it was found that the INS spectra calculated using the LDA agreed better with the experimental data than those obtained with the GGA, although the calculations using the GGA in the static approximation also showed a very good agreement with the INS measurements. Unlike INS, NCS measurements are sensitive to an integrated and cumulative response involving all vibrational modes affecting the motions of a particular atom. In this situation, one expects to be less sensitive to the details of the projected phonon density of states and their dispersive behavior. On the whole, our *ab initio* approach provides a convenient framework for the prediction of nuclear momentum distributions in solid-state systems, an observable also acessible via NCS measurements. Likewise, such a framework makes it possible to explore in a controlled and systematic fashion those features that contribute to the NCS line shape.

Proton kinetic energies in LiH obtained from NCS and INS experiments at 20 K and 300 K[11,40] are, within experimental error, equal to our *ab initio* results for the cubic LiH crystal

TABLE IV. Theoretical predictions for the (x,y,z) components of the Laplacian of the effective Born-Oppenheimer potential [cf. Eq. (24)] and isotropic average of the Laplacian, $\langle\nabla^2 V\rangle$. In the last two columns, PD denotes calculated values using phonon-dispersion relations [cf. Eq. (21)], whereas VDOS corresponds to the vibrational density of states [cf. Eq. (13)]. All values are give in units of meV Å^{-2}.

Nucleus	$\frac{\partial^2 V_n}{\partial x^2}$	$\frac{\partial^2 V_n}{\partial y^2}$	$\frac{\partial^2 V_n}{\partial z^2}$	$\langle\nabla^2 V\rangle_{PD}$	$\langle\nabla^2 V\rangle_{VDOS}$
H in LiH	7984	7652	7209	7622	7622
Li in LiH	8602	8137	7378	8055	8053
D in LiD	8033	7664	7202	7641	7642
Li in LiD	8641	8147	7377	8072	8070

TABLE V. Experimental values obtained for protons in LiH: average kinetic energies E_{kin}, square root of the second moment of the momentum distribution, σ, and the spherical average of the Laplacian of the effective Born-Oppenheimer potential, $\langle \nabla^2 V \rangle$, calculated within the isotropic 3D-HO approximation using Eq. (16).

T [K]	Method	E_{kin} [meV]	σ [Å^{-1}]	$\langle \nabla^2 V \rangle$ [meV Å^{-2}]
300	NCS[39]	76.0 ± 0.3	3.49 ± 0.05	7382 ± 423
20	NCS[39]	73.8 ± 0.3	3.44 ± 0.05	6968 ± 405
20	INS[40]	80 ± 1	3.59 ± 0.05	8265 ± 460

(at the time of writing, no experimental NCS data are available on solid crystalline LiD). We, therefore, find no evidence for the postulated broadening of the proton momentum distribution in solid LiH originating from a breakdown of the BOA.[5,6,41] The harmonic Born-Oppenheimer approximation in the ground electronic state provides a suitable framework to account for the ultrafast proton dynamics in solid LiH measured in NCS experiments.

The lack of observable non-BOA effects in the measured NCS spectra does not exclude that such effects indeed occur, yet at much more subtle a level than anticipated from previous theoretical predictions.[5,6,41] It must be stressed that the experimental values of the second moment of the proton momentum distribution in LiH have been obtained using a previous detector configuration of the VESUVIO spectrometer.[39,40] The overall resolution of the NCS method has been greatly improved since then, and new detectors are now available on VESUVIO.[42] The improved resolution of the new detector setup on the VESUVIO NCS spectrometer is capable of detecting smaller broadenings and/or shifts in the proton recoil peak than its predecessor, the EVS spectrometer, on which the LiH data used in this paper were measured.[39,40] This enhancement will, in principle, enable the detection of possible distortions of the proton momentum distribution due to the violation of the BOA under the weak-coupling regime.[5,6] In the weak-coupling regime, the excitation profile of the recoiling proton may lead to a series of small additional recoil peaks, arising from individual electronic excitations, which will be shifted from the position of the main recoil peak by their respective electronic excitation energies. This effect may lead to the emergence of an envelope of overlapping recoil peaks at higher energy-transfer values than those of the main proton recoil peak. The presence of a distribution of unresolved recoil features around the main proton recoil peak will result in a slight asymmetry toward higher energy transfers accompanied by a small shift of the main recoil peak toward lower energy transfers in order to satisfy the first-moment sum rule.[5,6] On the basis of our calculations, these effects will be quite small for LiH, amounting to a few percent of the overall NCS spectral width.

Improved experimental capabilities do not alone guarantee the successful detection of non-BOA effects in future experiments. A major difficulty is also related to the availability of reliable quantitative predictions of the detailed shape of the proton momentum distribution in the presence of non-BOA effects. Whereas it is relatively simple to predict peak shifts in energy transfer by resorting to tabulated values of electronic excitation energies (or by calculating them using *ab initio* methods), the real challenge resides in the quantitative prediction of the relative weights of the extra recoil peaks due to electronic excitations. Access to these spectral weights relies on the calculation of probabilities of individual excitations due to nonadiabatic couplings. This task constitutes a major challenge to current theoretical methods. For instance, an *ab initio* calculation of a static excitation within the Born-Oppenheimer approximation (e.g. using core-hole methods as implemented in the CASTEP package[30,31]) is not applicable in this situation owing to the intrinsic non-BOA nature of the excitation mechanisms proposed to date. Moreover, any time-dependent DFT or post-Hartree-Fock method is not applicable for the same reasons. More importantly, resorting to first-order perturbation theory to calculate the probabilities of individual electronic excitations[5,6] can only provide very rough numerical estimates for the expectation values of the perturbation between relevant excited electronic states.

At present, the only plausible *ab initio* method for the quantitative prediction of the distortion of proton momentum distributions seems to be an intrinsically non-BOA calculation. Towards this end, a very exciting and novel avenue for the *ab initio* prediction of nuclear momentum distributions has emerged in the last few years. An unprecedented increase in high-performance computing power and parallelization in computational quantum chemistry allows for *ab initio* electronic-structure calculations beyond the BOA approximation for small molecular systems.[43–47] These non-BOA calculations use explicitly correlated Gaussian basis functions with basis-set dimensions easily reaching the thousands. By employing the variational method, one can always ensure that total-energy minimization using the most flexible form of a basis set yields the best possible approximation (within a certain supercomputing capacity) to the non-BOA wave function for the system under investigation.[43]

In the context of the present paper, and as far as non-BOA effects in NCS measurements are concerned, proper account of non-BOA effects is always possible by recourse to explicitly correlated Gaussian basis functions. This situation does not always hold in calculations of non-BOA effects using first-order perturbation treatments[43] as the perturbation may be simply too large to handle.[43] Moreover, using non-BOA wave functions optimized from single-point energy calculations enables the calculation of numerous molecular properties,[43,45,46] including vibrational spectra.[44,47–49] Interestingly, familiar concepts, such as chemical bonding and molecular structure,[43] or dipole, quadrupole, and higher multipole moments,[46] have very different physical interpretations when the wave function simultaneously (and equivalently) depends on the coordinates of both nuclei and electrons.[43]

Ab initio calculations of vibrational spectra beyond the BOA have already been performed on isolated LiH[44] and LiH^+.[47] In principle, the nuclear kinetic energy in an isolated system can be obtained from these calculations. For an isolated LiH molecule, the average vibrational kinetic energy (the sum of vibrational kinetic energies for Li and H) in the ground rotovibrational state calculated from a Dunham-like expansion accounting for nonadiabatic effects yields a value of 43.185 meV.[44] This value can be contrasted with the total average vibrational kinetic energy calculated using the isolated molecule model.[27] In this model, the vibrational degrees

of freedom are treated quantum mechanically within the framework of the 3D-HO, and the translational and rotational degrees of freedom are treated classically based on the Sachs-Teller mass-tensor formalism. The value of the average vibrational kinetic energy for an isolated LiH molecule calculated from this model is 42.86 meV; thus, it is ca. 1% less than the value obtained from the Dunham formula. Due to the lack of similar quantitative predictions for the contributions of excited electronic states to the broadening of the nuclear momentum distribution, it is still not possible to assess whether additional broadening mechanisms can be expected due to non-BOA effects in NCS arising from the excitation mechanisms proposed by Gidopoulos,[5] Reiter and Platzman.[6] In this context, the *ab initio* calculation of nuclear momentum distributions via non-BOA approaches using explicitly correlated Gaussian basis functions with nonseparable electronic and nuclear coordinates remains an area to be explored. Clearly, *ab initio* non-BOA methods can at least be applied to the interpretation of NCS experiments on isolated diatomic molecules in the gas phase. Promising molecular systems include H_2, HF, and LiH, as well as their deuterated cousins.

Despite impressive achievements in the field of non-BOA electronic structure calculations during the last decade, the application of the method to condensed-matter systems still remains uncharted territory. Thus, further work must concentrate on two tasks: first, on choosing simple molecular systems as benchmarks, preferably in the gas phase, to assess the magnitude of non-BOA effects; and, second, on finding the most appropriate (albeit approximate) methods for the prediction of these effects in condensed-matter systems. For solid crystalline systems, like LiH and LiD, one may also focus on providing the best possible theoretical predictions of proton momentum distributions within the BOA in order to assess any discrepancies between tractable theoretical predictions and NCS measurements. Such an approach constitutes the main driving force behind this paper.

Resorting to DFT-based molecular dynamics (MD-DFT) methods can also be used to increase the accuracy of the calculation compared to the present harmonic calculations based on DFPT. In this context the path-integral MD-DFT method has been successfully implemented in the calculation of proton momentum distributions in water.[50] An even more accurate avenue for the calculation of proton momentum distributions has recently been proposed by Lin, Morrone, Car, and Parrinello.[51] The so-called displaced path integral molecular dynamics method is conceptually advantageous as it exploits the concept of nuclear effective force as the most fundamental (and physically appealing) observable. Studying the shape of the effective force along different crystallographic dimensions allows for the possibility of distinguishing between intrinsic anharmonic effects in the proton momentum distribution and non-Gaussian behavior arising from the anisotropy of the potential.[51] The method is also computationally advantageous and can be applied to compare *ab initio* predictions against experimental data in an intuitive manner.

VI. CONCLUSIONS

The widths of nuclear momentum distributions and the Laplacians of the effective Born-Oppenheimer potentials were modelled theoretically in solid LiH and LiD. To this end, we have resorted to *ab initio* PW-DFT computations using the GGA-PBE functional. Vibrational densities of states and phonon-dispersion curves were calculated from optimized unit-cell geometries. The calculations were based on the harmonic and Born-Oppenheimer approximations. Neither excited electronic levels nor time-dependent phenomena were taken into account.

On the whole, the harmonic Born-Oppenheimer approximation in the ground electronic state accounts very well for the measured nuclear momentum distributions in solid LiH. If non-BOA effects affect the proton momentum distribution in LiH, they manifest themselves at a much more subtle level than previously anticipated.

Further experiments and more elaborate theoretical modeling are in progress to shed more light on possible departures from the BOA in NCS experiments. These studies have important consequences in the further development of theoretical models describing proton momentum distributions in isolated molecules and condensed-matter systems.

ACKNOWLEDGMENTS

The authors gratefully acknowledge the UK Science & Technology Facilities Council for financial support and its e-Science facility for access to computing resources.

*matthew.krzystyniak@ntu.ac.uk

†Also at Department of Physics and Astronomy, University College London, Gower Street, London WC1E 6BT, United Kingdom.

[1] G. I. Watson, J. Phys. Condens. Matter **8**, 5955 (1996).

[2] C. Andreani, D. Colognesi, J. Mayers, G. F. Reiter, and R. Senesi, Adv. Phys. **55**, 377 (2005).

[3] V. F. Sears, Phys. Rev. B **30**, 44 (1984).

[4] C. A. Chatzidimitriou-Dreismann, T. Abdul-Redah, and B. Kolaric, J. Am. Chem. Soc. **123**, 11945 (2001).

[5] N. I. Gidopoulos, Phys. Rev. B **71**, 054106 (2005).

[6] G. F. Reiter and P. M. Platzman, Phys. Rev. B **71**, 054107 (2005).

[7] C. A. Chatzidimitriou-Deismann and M. Krzystyniak, Laser Phys. **20**, 990 (2010).

[8] R. Senesi *et al.*, Physica B **276**, 200 (2000).

[9] R. Senesi,D. Colognesi, A. Pietropaolo, and T. Abdul-Redah, Phys. Rev. B **72**, 054119 (2005).

[10] J. P. Perdew, K. Burke, and M. Ernzerhof, Phys. Rev. Lett. **77**, 3865 (1996).

[11] J. Boronat, C. Cazorla, D. Colognesi, and M. Zoppi, Phys. Rev. B **69**, 174302 (2004).

[12] T. Abdul-Redah, P. A. Georgiev, M. Krzystyniak, D. K. Ross, and C. A. Chatzidimitriou-Dreismann, Physica B **385**, 57 (2006).

[13]D. Colognesi, A. J. Ramirez-Cuesta, M. Zoppi, R. Senesi, and T. Abdul-Redah, Physica B **350**, E983 (2004).
[14]J. Mayers, C. Andreani, and G. Baciocco, Phys. Rev. B **39**, 2022 (1989).
[15]J. Mayers, Phys. Rev. B **41**, 41 (1990).
[16]J. Mayers, Phys. Rev. Lett. **71**, 1553 (1993).
[17]C. Andreani, D. Colognesi, and E. Pace, Phys. Rev. B **60**, 10008 (1999).
[18]J. Mayers and T. Abdul-Redah, J. Phys. Condens. Matter **16**, 4811 (2004).
[19]G. B. West, Phys. Rep. C **18**, 263 (1975).
[20]A. C. Evans, D. N. Timms, J. Mayers, and S. M. Bennington, Phys. Rev. B **53**, 3023 (1996).
[21]A. L. Fielding, D. N. Timms, and J. Mayers, Europhys. Lett. **44**, 255 (1998).
[22]S. W. Lovesey, *Theory of Neutron Scattering from Condensed Matter* (Clarendon, Oxford, 1984).
[23]B. E. Wilson, J. C. Decius, and P. C. Cross, *Molecular Vibrations, The Theory of Infrared and Raman Vibrational Spectra* (Dover Publications, New York, 1980).
[24]P. C. H. Mitchell, S. F. Parker, A. J. R. Cuesta, and J. Tomkinson, *Vibrational Spectroscopy with Neutrons* (World Scientific, Singapore, 2005).
[25]S. Baroni, S. de Gironcoli, A. dal Corso, and P. Giannozzi, Rev. Mod. Phys. **73**, 515 (2001).
[26]D. Colognesi, E. Degiorgi, and E. Pace, Physica B **293**, 317 (2001).
[27]M. Krzystyniak, J. Chem. Phys. **133**, 144505 (2010).
[28]J. Boronat, C. Cazorla, D. Colognesi, and M. Zoppi, Phys. Rev. B **69**, 174302 (2004).
[29]V. F. Sears, Phys. Rev. A **7**, 340 (1973).
[30]M. D. Segall, P. J. D. Lindan, M. J. Probert, C. J. Pickard, P. J. Hasnip, S. J. Clark, and M. C. Payne, J. Phys. Condens. Matter **14**, 2717 (2002).
[31]K. Refson, P. R. Tulip, and S. J. Clark, Phys. Rev. B **73**, 155114 (2006).
[32]J. P. Perdew, J. A. Chevary, S. H. Vosko, K. A. Jackson, M. R. Pederson, D. J. Singh, and C. Fiolhais, Phys. Rev. B **46**, 6671 (1992).
[33]M. Ernzerhof and G. E. Scuseria, J. Chem. Phys. **110**, 5029 (1999).
[34]J. P. Perdew, K. Burke, and M. Ernzerhof, Phys. Rev. Lett. **77**, 3865 (1996).
[35]M. J. van Setten, V. A. Popa, G. A. de Wijs, and G. Brocks, Phys. Rev. B **75**, 035204 (2007).
[36]E. Staritsky and D. Walker, Anal. Chem. **28**, 1055 (1956).
[37]J. L. Martins, Phys. Rev. B **41**, 7883 (1990).
[38]G. D. Barrera, D. Colognesi, P. C. H. Mitchell, and A. J. Ramirez-Cuesta, Chem. Phys. **317**, 119 (2005).
[39]T. Abdul-Redah, P. Georgiev, M. Krzystyniak, D. Ross, and C. Chatzidimitriou-Dreismann, Physica B **385**, 57 (2006).
[40]D. Colognesi, A. Ramirez-Cuesta, M. Zoppi, R. Senesi, and T. Abdul-Redah, Physica B **350**, E983 (2004).
[41]I. E. Mazets, C. A. Chatzidimitriou-Dreismann, and G. Kurizki, in *Decoherence, Entanglement and Information Protection in Complex Quantum Systems*, edited by V. M. Akulin, A. Sarfati, G. Kurizki, and S. Pellegrin (Springer, Dordrecht, 2005), Vol. 189, p. 549.
[42]S. Imberti and C. E. A. Andreani, Nucl. Instrum. Methods Phys. Res., Sect. A **552**, 463 (2005).
[43]S. Bubin and L. Adamowicz, J. Chem. Phys. **126**, 214305 (2007).
[44]S. Bubin, L. Adamowicz, and M. Molski, J. Chem. Phys. **123**, 134310 (2005).
[45]S. Bubin and L. Adamowicz, J. Chem. Phys. **121**, 6249 (2004).
[46]M. Cafiero and L. Adamowicz, Phys. Rev. Lett. **88**, 033002 (2002).
[47]M. Stanke, S. Bubin, and L. Adamowicz, Phys. Rev. A **79**, 060501 (2009).
[48]S. Bubin, F. Leonarski, M. Stanke, and L. Adamowicz, J. Chem. Phys. **130**, 124120 (2009).
[49]S. Bubin, F. Leonarski, M. Stanke, and L. Adamowicz, Chem. Phys. Lett. **447**, 12 (2009).
[50]J. A. Morrone, V. Srinivasan, D. Sebastiani, and R. Car, J. Chem. Phys. **126**, 234504 (2007).
[51]L. Lin, J. A. Morrone, R. Car, and M. Parrinello, Phys. Rev. Lett. **105**, 110602 (2010).